International Journal of Heat and Mass Transfer 96 (2016) 438–450

Contents lists available at ScienceDirect

International Journal of Heat and Mass Transfer

journal homepage: www.elsevier.com/locate/ijhmt

Theoretical analysis and experiment on gas film temperature in a spiral groove dry gas seal under high speed and pressure

Xuexing Ding, Junjie Lu *

College of Petrochemical Engineering, Lanzhou University of Technology, Lanzhou 730050, Gansu, China

ARTICLE INFO

Article history:
Received 14 October 2015
Received in revised form 31 December 2015
Accepted 19 January 2016
Available online 4 February 2016

Keywords:
Dry gas seal
Face seals
Temperature monitoring
Thermal dissipation analysis
Temperature distribution

ABSTRACT

Experimental tests are conducted in this study to determine the temperature distribution in a dry gas seal by establishing a temperature field test system and choosing sensors that are stable for extreme operating conditions. The temperatures of a narrow gap-occurring gas film with seal rings under different rotating speeds and pressures are measured, and a theoretical method is developed to compare the temperature data. A theoretical procedure based on the compressible Reynolds equation and energy equation considering thermal dissipation is used to explore the temperature distribution in the gas film. The results obtained from the experimental data and thorough theoretical calculations are consistent. The temperature distribution in the gas film face shows the following order: root radius temperature > inner radius > outer radius. Increases in temperature are attributed to thermal dissipation caused by a significant pressure drop in the root radius region. A seal isothermal model is compared with the thermal model and values of the sealing opening force and leakage flow in the thermal model are greater than the values in the isothermal model. Thus, the results of this research reveal that the proposed theoretical calculation method can be applied to analyze dry gas seal temperatures and that thermal dissipation is a significant factor that may be used to optimize groove designs in the future.

1. Introduction

The use of spiral groove dry gas seals has been expanded from low to high speed and high pressure. To suit operating conditions, such seals are subjected to high load. The temperature rise caused by thermal dissipation and friction heat is induced by a significant pressure drop. Moreover, high temperature gradients alter the thermal stresses in seal rings; this change may cause thermal deformation in seal rings. As a result of seal ring deformation, gas film thickness is so asymmetrical that the flow changes. What is worse, the gas film stiffness decreases and the leakage of dry gas seal increases. Thus, the stability and performance of seal system decreases.

Many works have been conducted recently on the theoretical and experimental problems with seal face temperature.

Li [1] used finite element method to set a heat value on seal interfaces for the energy equation and determined the temperature distribution in seal rings. Luan et al. [2] referenced Buck's simplified model and considered thermal changes in seal rings. Doane et al. [3] designed experimental test technology to illustrate the property of the thermal boundary condition for a mechanical seal. Merati et al. [4] researched temperature distribution in a turbulence flow field via computational fluid dynamics. Tournerie and Brunetière [5–7] theoretically and experimentally studied the temperature distributions between the film and the rings, specifically, the influence between temperature and seal performance. Faria et al. [8] noted that face temperature fields are affected by seal groove shape. Offermann et al. [9] identified the influence of thermo-elastic on the load in accordance with thermo-elastic deformation theory. Thomas [10] focused on the thermo-elasto-hydrodynamic (TEHD) problem and applied a numerical solution to address the thermal transfer that results in the thermal deformation of seal rings. Andres et al. [11] analyzed the leakages of three different types of gas seals under high temperature. Blasiak et al. [12] established a three-dimensional thermodynamics model of a seal face to determine the temperature distribution in non-contacting liquid film seals. Wang et al. [13] analyzed the thermal fluid in dry gas seals under high temperature and gas cooled condition through simulation. Etsion et al. [14] monitored a non-contacting mechanical sealing stationary ring in their experimental study on performance of dry gas seals. Kasem et al. [15,16] tracked transient temperature changes continuously. Huang et al. [17,18] identified the performance parameters of dry gas seals through

* Corresponding author.
E-mail addresses: dingxx1@163.com (X. Ding), loveljj4566@163.com (J. Lu).

http://dx.doi.org/10.1016/j.ijheatmasstransfer.2016.01.045
0017-9310/

Nomenclature

n_r	rotating speed, r/min
R_i	inner radius, m
R_o	outer radius, m
p_i	environmental pressure, MPa
p_o	medium pressure, MPa
kn'	Knudsen number
U_0	linear velocity of the inner radius of a seal ring, m/s
χ	compressible correction coefficient under slip boundary condition
Λ	compressible coefficient
ζ	non-dimensional polar radius
r	seal ring radius, m
E	half of groove depth, m
P	non-dimensional gas film pressure
h	lubrication film thickness, m
H	non-dimensional lubrication film thickness
δ	gas film thickness, m
σ_v	coefficient of the adjustment in the molecular tangential momentum
R_e	slip radius, m
b	seal ring face width, m
A_s	stationary ring area, m^2
A_e	effective area of medium acting on the stationary ring surface, m^2
a	coefficient of linear expansion for stationary ring, 1/K

Integration constant

A_i	$i = 1, 2, 3$
B_i	$i = 1, 2, 3$
n	number of spiral grooves
β_0	groove coefficient
ε	small parameter of iterative perturbation
q	density of thermal flux, W/m^2
Φ	thermal flux, W
p	pressure of gas film, MPa
φ	non-dimensional polar angle
ψ	PH non-dimensional function
η	ratio of groove depth
ω	equivalent spiral angle
l	molecular free path, m
T	gas film temperature, °C
u	circumference velocity of gas film, m/s
c_p	specific heat of gas at constant pressure, kJ/(kg K)
μ	dynamic viscosity of gas, Pa s
v	radial velocity of gas film, m/s
λ	heat conductivity, W/(m K)
α	spiral angle, rad
ρ	gas density, kg/m^3
L	axial length of stationary ring, m
F_s	spring force, N
T_0	initial temperature, K
δ_{ta}	thermo-elastic deformation
c_{ij}	$i = 1, 2$ and $j = 0, 1$
c'_{ij}	$i = 1, 2$ and $j = 0, 1$

the acoustic emission monitoring method by installing sensors on the face of a seal ring. Luan [19,20] facilitated the conjugate thermal transfer of turbulent or laminar flow in a mechanical seal by performing numerical calculations that considered thermal generation, conduction, and convection. Visconte et al. [21] described an experimental methodology to measure leakage flow in an air-lubricated seal and compared testing data via CFD. Blasiak [22] proposed a mathematical model and analyzed the effect of parameters on the temperature fields in a non-contacting face seal.

These works followed a process to thermally analyze seals but neglected the effect of thermal dissipation on the temperature distribution in gas films. The present study represents the first attempt to calculate gas film temperature in consideration of thermal dissipation by using the new test technology for dry gas seals. The test technology for gas film temperature is difficult to implement in dry gas seal under high speed and high pressure because the clearance of the seal faces is only 3–5 μm. This work examines micro-scale gas film temperature to determine temperature field distribution in gas films by establishing a temperature field test system for dry gas seals with LABVIEW, and then by choosing sensors that are stable for high operating conditions, by implementing interference suppression measures, and by measuring gas film temperature. The test data are compared based on the velocity slip boundary condition and gas film pressure in combination with the thermal dissipation energy equation for gas films in dry gas seals; this comparison facilitates the determination of temperature field distribution in gas films. And it explores the variation of the values of the sealing opening force and leakage flow between a seal isothermal model and the thermal model employed in the passage. The results clarify the concept of gas film temperature and guide the design of dry gas seals significantly.

2. Experimental test

2.1. Test bench system

A test bench with a spiral groove dry gas seal is used in the test experiments [Fig. 1(a)]. This bench includes four major components, namely, a transmission, seal, gas supply, and test system, as illustrated in Fig. 1(b). The transmission system consists of an axle, a variable frequency motor, a gearbox, and a control cabinet; this system can operate from 0 r/min to 16,500 r/min. The seal system that serves as the research object in this study is a spiral groove dry gas seal with double faces [Fig. 2(a)]; the gas supply system is a supporting facility for this seal system. The test system consists of hardware devices and software; the former comprises thermal sensors and data acquisition units, among others, and the software used is LABVIEW.

2.2. Test technology

2.2.1. Selection and placement of thermal sensors

The rotating ring is composed of a hard alloy and can rotate at high speed. Therefore, the temperature distribution of the rotating ring face possesses coaxiality. Temperature is distributed along the radial position of the rotating ring, and the variation in temperature at three positions on the rotating ring face can be measured by three-channel temperature sensors considering the outer, root,

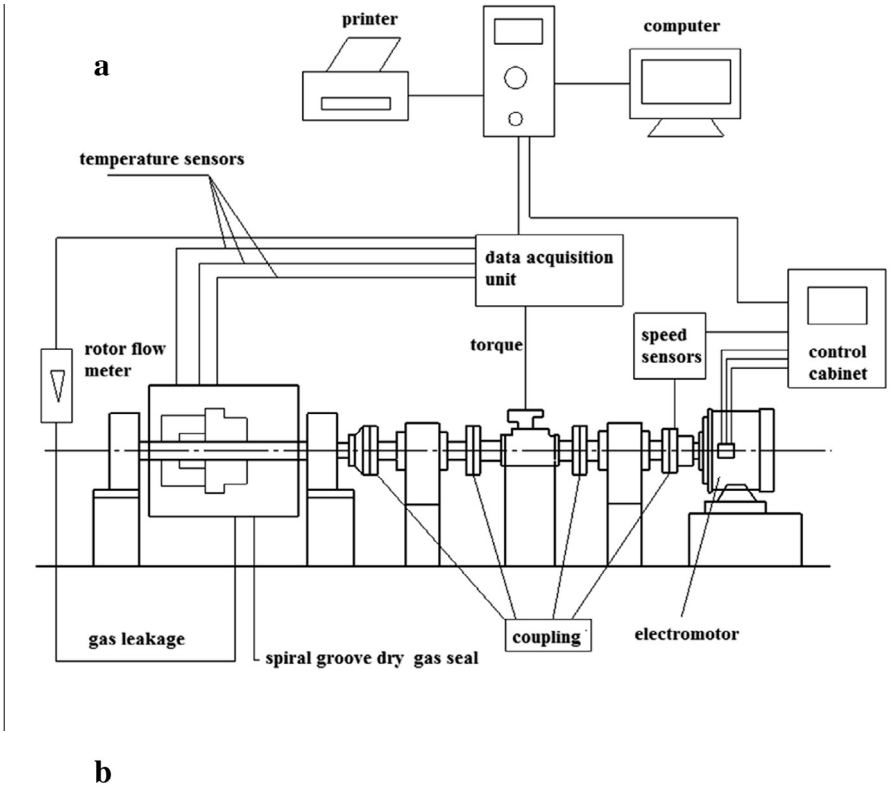

Fig. 1. (a) Schematic and (b) photograph of the test bench.

and inner radii of the rotating ring. The three temperature sensors are placed 120° from one another because the face is narrow [Fig. 2 (b)]. Temperatures are recorded by sending the signal received by the sensors to the Taiwan Advantech ADAM-4051 temperature collecting card.

Because the clearance of the stationary and rotating rings is micron-scale, generating an accurate response to temperature variations is difficult when using ordinary sensors because of the high speed and pressure in the system. Therefore, the temperature sensor Model Pt100 M 222 20NIPt6 is used in this study; this sensor contains a German Heraeus 1/3B level chip and platinum thermistor. The acceptable temperature range of this sensor is −50 °C to 450 °C, and the stability of the R0 drift is less than or equal to 0.04% (450 °C after 1000 h). The thermal response time is 0.1 s. The placements of the sensors are described by special punches corresponding to the surfaces of the outer, root and inner radii of the rotating ring. The three positions are separated from one another by 120°; similarly, the three holes are separated at angles of 120°

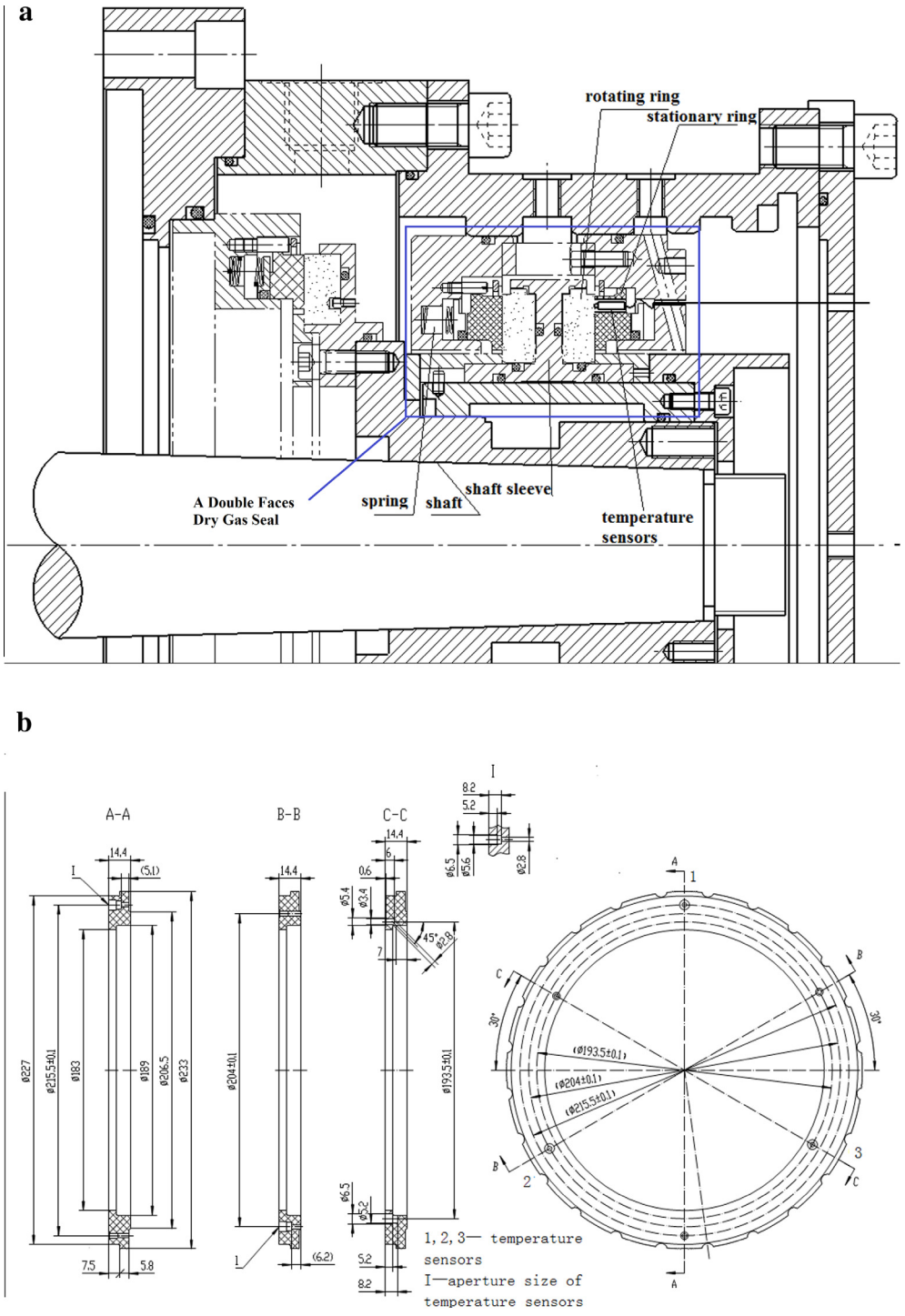

Fig. 2. (a) Test bench and (b) static ring on which sensors are placed.

with distances of 96.75, 102.00, and 107.75 mm from the center of the stationary ring, as shown in Fig. 2(b). These three holes must correspond to the wafer on the rotating ring. Three cylindrical probes are subsequently installed in the holes in the stationary ring.

2.2.2. Anti-jamming measurement

Several equipment, such as a motor and air compressor, among others, are located near the test bench. As the interference of the electromagnetic energy may affect the sensors, the following anti-jamming measures are implemented:

(1) Grounding technology is used to damp the interference.
(2) The length of the conducting wire is minimized, and a high-density shielding copper grid is used.
(3) The test bench, test instrument, and computer are placed near each other to improve the anti-interference performance of the transmission channel.
(4) A high-input impedance collecting card (the input impedance is increased from 10 M to 1 G) is customized to ensure that the interference current exerts no effect on the incoming signal.

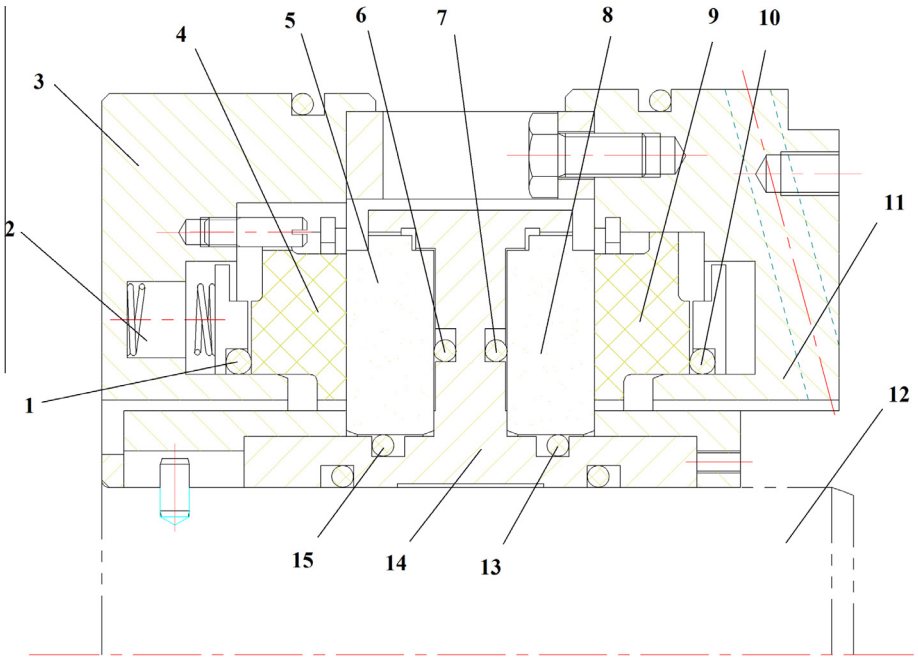

1, 6, 7, 10, 13, 15: O-rings; 2: Springs; 3, 11: Seal chambers;
4, 9: Stationary rings; 5, 8: Rotating rings; 12: Axle; 14: Axle sleeve

Fig. 3. Schematic of the spiral groove seal system.

(5) The collecting card adopts two-sided input (a one-channel signal is inputted into positive and negative channels) to limit common-mode interfering signals and enhance the anti-interference performance of the test equipment.

Because temperature test is complex. The test bench is improved to anti-jamming, optimize operating conditions, and improve measurement precision.

2.3. Test procedure

The seal system is installed in the head of the output axle. According to the experimental scheme, a spiral groove dry gas seal is selected as the seal system. Fig. 3 presents a schematic of the spiral groove seal system. The seal system mainly consists of springs, O-rings, and stationary and rotating rings. The springs and stationary rings are installed in the stationary ring seats and the second seal is sealed by the O-ring. The rotating ring is fixed on the axle sleeve and rotated by the axle, and the surface of the rotating ring features a series of spiral grooves. The seal is a double-faced seal [Fig. 2(a)] to allow easy assembly and disassembly. The gas supply system provides pressure to the seal system. The inlet gas pressure is controlled by adjusting the gas intake valve from 0 to 4.0 MPa, and the inlet gas pressure is read by using a gas pressure gauge. Temperature sensors signals are transformed as physical signal, after which the digital signal is realized by data acquisition. The digital signal is transmitted to a computer and displayed in output equipment.

The monitoring system is built using LabVIEW software. The sampling rate is decided by the A/D conversion, computer storage, and sampling scope. On the one hand, if the period of sampling is too low, the data requires a large storage. On the other hand, if the period of sampling is too large, the data may become distorted. Thus, the temperature sampling rate for the PC monitoring system is set to once per second.

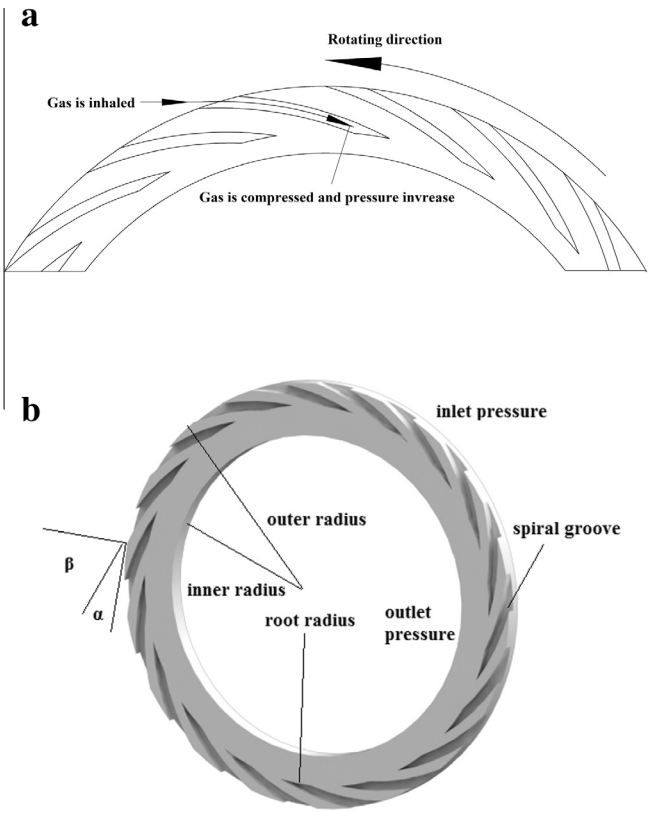

Fig. 4. (a) Operating principle and (b) schematics of the spiral groove seal rotating ring.

During testing, the rotating speed is maintained at 10,000 rpm and the inlet gas pressure is increased by increments of 0.5 MPa from 2.0 MPa to 4.0 MPa using the gas supply system. The available

temperature data are measured at the inner, root, and outer radii. Then, the inlet gas pressure is maintained at 3.0 MPa and the rotating speed is increased at increments of 1000 r/min from 8000 r/min to 10,000 r/min. The run time of different operating conditions is controlled to 141 s. The run time of every operating condition is decided by three aspects: the dry gas seal must be rebalanced from one operating condition to another, the response time of the thermal sensors, and to prevent the temperature curves of the three seal radii from assuming a single curve because of temperature averaging. Experiments performed under the given conditions are repeated twice to guarantee the reliability of the results.

3. Theoretical model

3.1. Spiral groove seal mechanism

Fig. 4(a) presents the operating principle of a spiral groove seal rotating ring. The seal gas is bubbled into the seal chamber. When the rotating ring is switched on, the gas proceeds into the spiral groove of the rotating ring in the circumferential direction. The gas then moves to the groove root and is constantly compressed. During gas movement, the pressure of the gas in the spiral groove increases so that an opening force is produced. The stationary ring is pushed by the rotating ring. The springs and the back pressure of the gas generate a closing force on the stationary seal rings in the axial direction. Thus, a gas film is formed between the seal faces, and the gas film thickness reaches 3–5 μm. Any leakage present is sealed by the gas film. The schematics of a spiral groove seal rotating ring is established in Fig. 4(b) to analyze the gas film dynamics; here, α is the spiral angle, n_r is the rotating speed, R_i is the inner radius, R_o is the outer radius, p_i is the environmental pressure, and p_o is the medium pressure.

3.2. Gas film dynamics

It is assumed that the gas exhibits laminar flow, a continuous medium, and steady-state flow. The micro flow of the gas film is similar to that of a rarefied gas. Thus, boundary slippage is essential for the performance of the dry gas seal. The Reynolds equation considering slip boundary conditions can be written as follows [23]:

$$\frac{\partial}{\partial\varphi}\left[\frac{ph^3}{\mu}(1+6kn')\frac{\partial p}{\partial\varphi}\right]+\frac{\partial}{\partial R}\left[\frac{ph^3}{\mu}(1+6kn')\frac{\partial p}{\partial R}\right]=6U_0\frac{\partial(ph)}{\partial\varphi} \quad (1)$$

where $kn'=l'/h$ is the Knudsen number with $10^{-3}\le kn'\le 10^{-1}$, $U_0=2\pi n_r R_i$ is the linear velocity of the inner radius of the seal ring, μ is the dynamic viscosity of gas, p is the pressure of the gas film, δ is the gas film thickness and φ is the non-dimensional polar angle.

Eq. (1) is computed using the non-dimensional method, and the new equation is expressed as:

$$\frac{\partial}{\partial\varphi}\left[PH^3\frac{\partial P}{\partial\varphi}\right]+\frac{\partial}{\partial\zeta}\left[PH^3\frac{\partial P}{\partial\zeta}\right]=\chi\frac{\partial(PH)}{\partial\varphi} \quad (2)$$

where $\chi=\Lambda/(1+6kn')$ is the compressible correction coefficient under slip boundary conditions, $\Lambda=\frac{12\pi\mu n_r R_i^2}{p_i(\delta+E)^2}$ is the compressible coefficient, $P=p/p_i$ is the non-dimensional gas film pressure, $\zeta=r/R_i$ is the non-dimensional polar radius, r is the seal ring radius, E is half of the groove depth, H is the non-dimensional lubrication film thickness, δ is the gas film thickness, and φ is the non-dimensional polar angle.

The PH linear method is employed in combination with the iteration method to solve Eq. (2) (non-linear Reynolds equation). The PH linear method considers that the nonlinear partial differential equation can be converted into a linear partial differential equation; the analytical solution of the distribution of gas dynamic pressures in the spiral groove may be roughly obtained. Using the PH linear method, a possible solution to the Reynolds equation is obtained, and the relationship between gas film temperature and pressure is determined. The equation of the gas film pressure is as follows [23]:

$$P=\psi_2/H=1+\eta\left(\eta_{1(\zeta)}\cos\omega+\eta_{2(\zeta)}\sin\omega\right)\Big/H-\frac{3}{2}\beta_0\eta^2\eta_{2(\zeta)}(\zeta_0-\zeta) \quad (3)$$

where

ψ is the PH non-dimensional function,
$\eta=E/(E+h)$,
$h=H(\delta+E)$, and
$\zeta_0=R_0/R_i$

$$\eta_{1(\zeta)}=c_{10}e^{\sqrt{\beta_1}\zeta}+c'_{10}e^{-\sqrt{\beta_1}\zeta}+\left(c_{11}e^{\sqrt{\beta_1}\zeta}+c'_{11}e^{-\sqrt{\beta_1}\zeta}+\frac{A_1}{2\sqrt{\beta_1}}\zeta e^{\sqrt{\beta_1}\zeta}-\frac{B_1}{2\sqrt{\beta_1}}\zeta e^{-\sqrt{\beta_1}\zeta}\right)\varepsilon$$

$$\eta_{2(\zeta)}=c_{20}e^{\sqrt{\beta_1}\zeta}+c'_{20}e^{-\sqrt{\beta_1}\zeta}+\left(c_{21}e^{\sqrt{\beta_1}\zeta}+c'_{21}e^{-\sqrt{\beta_1}\zeta}+\frac{A_2}{2\sqrt{\beta_1}}\zeta e^{\sqrt{\beta_1}\zeta}-\frac{B_2}{2\sqrt{\beta_1}}\zeta e^{-\sqrt{\beta_1}\zeta}-\frac{\alpha_2}{\beta_1}\right)\varepsilon$$

$$\beta_1=\beta_0^2+n^2$$

where h is the lubrication film thickness, H is the non-dimensional lubrication film thickness, δ is the gas film thickness, β_0 is the groove coefficient, and n is the number of spiral grooves. As well, A_i, where $i=1,2,3$; B_i, where $i=1,2,3$; c_{ij}, where $i=1,2$ and $j=0,1$; and c'_{ij}, where $i=1,2$ and $j=0,1$, are the integration constants, ε is the small parameter of iterative perturbation, η is the ratio of the groove depth, and ω is the equivalent spiral angle.

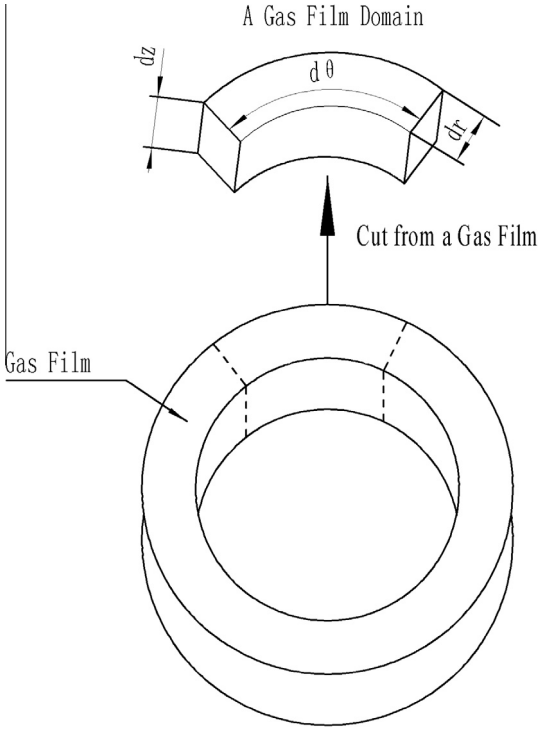

Fig. 5. A controlled volume of the gas film.

3.3. Thermal dissipation analysis

Fig. 5 displays the energy model for a controlled volume of the gas film. Heat convection and diffusion passes the model. Temperature fluctuations occur in the radial, circumferential, and film thickness directions. Of these, circumferential temperature fluctuations can be neglected because of the rotating speed. Thus, only the thermal energy in the radial and film thickness directions is studied here.

The equation for thermal diffusion in the radial direction is expressed as:

$$d\Phi_{\lambda,r} = q_{\lambda,r} r d\theta = -\lambda \frac{\partial T}{\partial r} r d\theta \tag{4}$$

$$d\Phi_{\lambda,r+dr} = q_{\lambda,r+dr}(r+dr)d\theta = -\lambda \frac{\partial}{\partial r}\left(T + \frac{\partial T}{\partial r}dr\right)(r+dr)d\theta \tag{5}$$

The equation for thermal convection in the radial direction is written as:

$$d\Phi_{h,r} = q_{h,r} r d\theta = \rho v c_p T r d\theta \tag{6}$$

$$\begin{aligned} d\Phi_{h,r+dr} &= q_{h,r+dr}(r+dr)d\theta \\ &= \rho c_p \left(v + \frac{\partial v}{\partial r}dr\right)\left(T + \frac{\partial T}{\partial r}dr\right)(r+dr)d\theta \end{aligned} \tag{7}$$

Referring to Eqs. (4) and (5), the energy equation of micro-control with thermal diffusion per unit time is expressed as:

$$d\Phi_{\lambda} = \lambda \frac{\partial T}{\partial r} dr d\theta + \lambda r \frac{\partial^2 T}{\partial r^2} dr d\theta \tag{8}$$

Based on Eqs. (6) and (7), the energy equation of micro-control with heat convection per unit time is written as:

$$d\Phi_h = -\rho c_p v T dr d\theta - \rho c_p v r \frac{\partial T}{\partial r} dr d\theta - \rho c_p T r \frac{\partial v}{\partial r} dr d\theta \tag{9}$$

A new heat factor (the dissipation of viscous fluid) should be considered during micro-control. The expression of thermal dissipation [24] is expressed as:

$$\dot{\Phi} = \frac{2\mu}{R_i^2}\left(\frac{\partial u}{\partial \varphi}\right)^2 + 2\mu\left(\frac{\partial v}{\partial r}\right)^2 \tag{10}$$

Thermal convection in the film thickness direction can be neglected because the gas film thickness is only 3–5 μm. The energy equation of a gas film with energy diffused in the film thickness direction is written as:

$$d\Phi_{\lambda} = \lambda \frac{\partial^2 T}{\partial r^2} dr d\theta \tag{11}$$

When combined with Eqs. (8)–(11), the principle of energy conservation indicates that the energy differential equation for gas film can be expressed as:

$$\begin{aligned} \rho c_p \left(vT + vr\frac{\partial T}{\partial r} + Tr\frac{\partial v}{\partial r}\right) &= \lambda\left(\frac{\partial T}{\partial r} + r\frac{\partial^2 T}{\partial r^2} + \frac{\partial^2 T}{\partial z^2}\right) \\ &+ \frac{2\mu}{R_i^2}\left(\frac{\partial u}{\partial \varphi}\right)^2 + 2\mu\left(\frac{\partial v}{\partial r}\right)^2 \end{aligned} \tag{12}$$

where T is the gas film temperature, ρ is the gas density, u and v are the respective circumferential and radial velocities of the gas film, c_p is the specific heat of the gas at constant pressure, λ is the thermal conductivity, μ is the dynamic viscosity of the gas, Φ is the thermal flux, and q is the density of the thermal flux.

Expressions for the circumferential and radial velocities of gas films [25] are written as:

$$\begin{cases} u = \frac{1}{2\mu R_i}(z^2 - Hz - hl')\frac{\partial p}{\partial \varphi} + U_0\left(1 - \frac{z+l'}{h}\right) \\ v = \frac{1}{2\mu R_i}(z^2 - Hz - hl')\frac{\partial p}{\partial \zeta} \end{cases} \tag{13}$$

where l is the molecular free path, σ_v is the coefficient of molecular tangential momentum adjustment, and $l' = (2 - \sigma_v)l/\sigma_v$.

4. Results and discussion

4.1. Experimental test result

4.1.1. Temperature distribution of the gas film under different pressure

Fig. 6 illustrates the effect of medium pressure on the temperature distribution along the rotating ring face when the rotational speed is 10,000 r/min. The temperature data are processed and plotted against the medium pressure, as shown in Fig. 7 (here, p_i represents medium pressures of 2.0, 2.5, 3.0, 3.5, and 4.0 MPa). The temperature increases by approximately 1.0 °C between 2.0 and 2.5 MPa, by 1.8 °C between 2.5 and 3.0 MPa, by 1.1 °C between 3.0 and 3.5 MPa, and by 2.9 °C between 3.5 and 4.0 MPa. The temperature of the rotating ring face also increases; this face is composed of the outer, root, and inner radii areas. The variation tendency of temperature in the rotating ring face is consistent. Fig. 6 also shows that temperature consistently peaks at the root radius and that the temperature in the inner radius is higher than that in the outer radius. The linear velocity of the outer radius is greater than that of the inner radius; thus, the flow within the outer radius of a rotating ring can rapidly remove increased heat in the system. The temperature increases with pressure until the former peaks at 90.90 °C at the root radius of the rotating ring (the maximum pressure is 4 MPa). As a result, heat is transmitted from the source to the rotating ring face by heat conduction.

4.1.2. Temperature distribution of the gas film under different rotating speed

Fig. 8 illustrates the effect of rotating speed on temperature distribution along the rotating ring face when the medium pressure is 3.0 MPa. The temperature data are processed and plotted against rotating speed, as shown in Fig. 9 (here, n_r is the rotating pressure at 8000, 9000, and 10,000 r/min). The temperature increases speed by approximately 10 °C between 8000 and 9000 rpm and by 7 °C between 9000 and 10,000 r/min. The temperature of the rotating ring face also increases; this face is composed of the outer, root, and inner radii. The variation tendency of temperature in the rotating ring face is consistent. The temperature increases faster under different rotating speeds than under different medium gas pressures, which illustrates that the effect of rotating speed on temperature is greater that of medium gas pressure. Fig. 8 also shows that the temperature consistently peaks at the root radius and that the temperature in the inner radius is higher than that in the outer radius. Thus, the flow within the outer radius of a rotating ring can rapidly eliminate increases in heat. As a result, heat is transmitted from the source to the rotating ring face by heat conduction. As the operating conditions become more extreme, the gas film temperature rises with increasing speed, which means the effect of operating conditions on the film temperature is obvious.

4.2. Comparison and verification of results

To prove the reliability of the experimental results, thermal dissipation in the gas film is calculated theoretically to determine the temperature distribution in the rotating ring face. First, the gas film pressure of the spiral groove is measured. The materials comprising the stationary and rotating rings are carbon graphite and hard alloy, respectively. The gas inlet and outlet pressures are set to the corresponding experimental supply pressures. Table 1 presents the

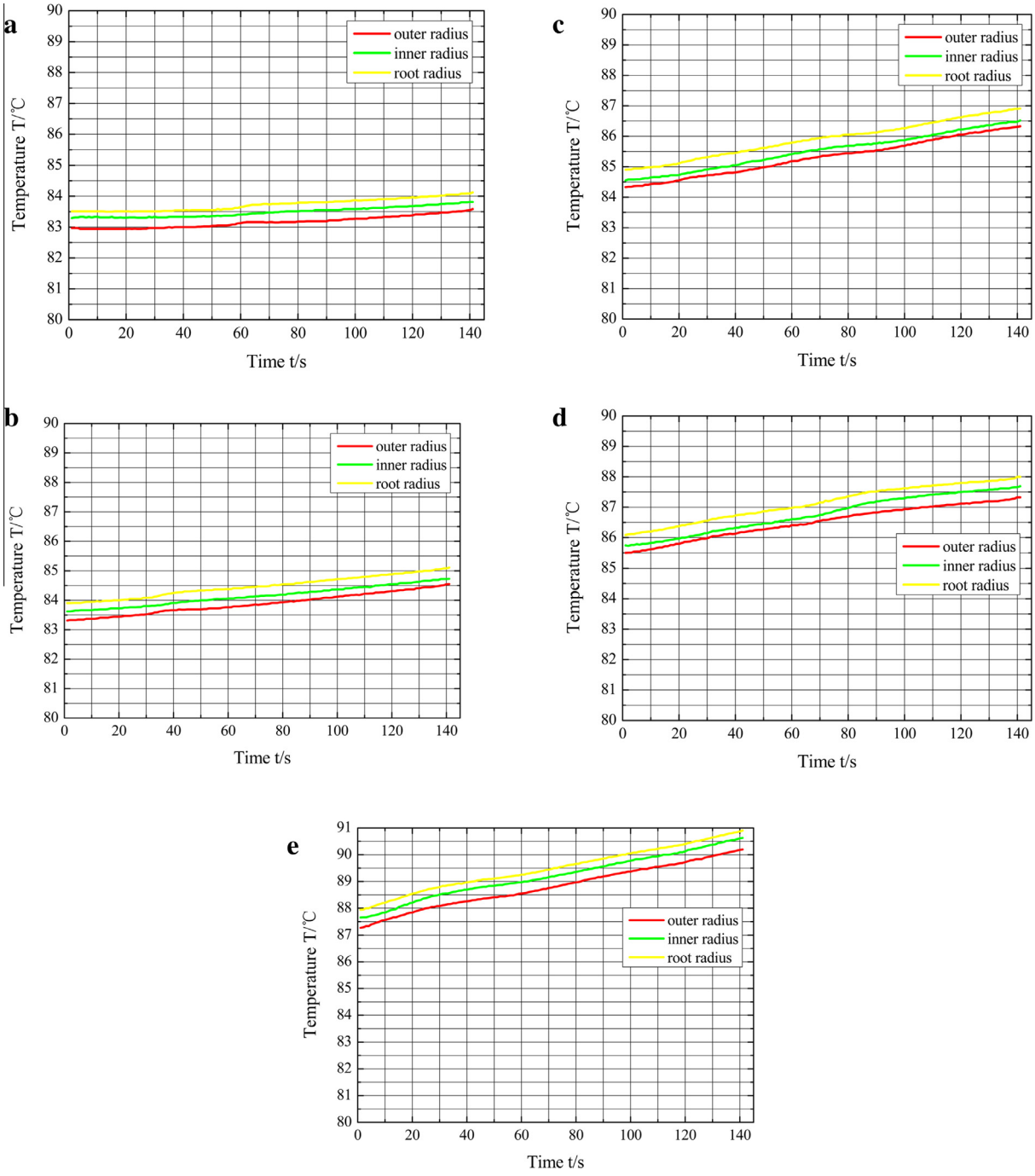

Fig. 6. Curves of temperature variation on the seal gas film for different pressure. (a) Temperature distribution at $p = 2.0$ MPa and $n = 10{,}000$ r·min^{-1}. (b) Temperature distribution at $p = 2.5$ MPa and $n = 10{,}000$ r·min^{-1}. (c) Temperature distribution at $p = 3.0$ MPa and $n = 10{,}000$ r·min^{-1}. (d) Temperature distribution at $p = 3.5$ MPa and $n = 10{,}000$ r·min^{-1}. (e) Temperature distribution at $p = 4.0$ MPa and $n = 10{,}000$ r·min^{-1}.

parameter values of the seal rings as well as the operating conditions of the experimental system.

The data in Table 1 are substituted into Eq. (3) and combined using MAPLE software. The pressure curve of the gas film is plotted against the non-dimensional radius, $\zeta = r/R_i$, where r and R_i are the radial locations of interest from the inner to the outer radius of the rotating ring and the inner radius of the rotating ring, respectively (Fig. 10). A pressure drop primarily occurs near the root radius of the rotational ring, which suggests that the maximum pressure point occurs at the root radius region. The maximum pressure is related to the maximum temperature during the experimental measurement. Results reveal that the temperature mainly increases because a significant drop in the pressure of the root radius region causes heat to dissipate over the face. This decrease in pressure accelerates thermal dissipation.

Fig. 10 depicts the pressure distribution along the seal radial direction and investigated through the least-square methods using MAPLE software. The expression of the gas film pressure may be written as:

$$P = 539.83757\zeta^4 - 2366.04907\zeta^3 + 2937.46759\zeta^2 - 515.75603\zeta - 594.52472 \quad (14)$$

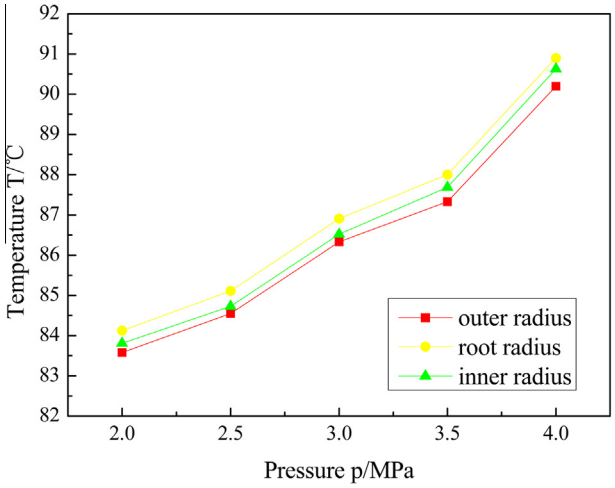

Fig. 7. Gas film temperature distribution at p = 2.0–4.0 MPa and n = 10,000 r·min^{-1}.

Table 2 lists physical constant related to the dry gas seal. The expression for the gas film with thermal dissipation can be obtained by substituting the physical constants derived in Eqs. (13) and (14) into Eq. (12). Therefore, the nonlinear second-order inhomogeneous differential equation with variable coefficients is computed as follows:

$$\frac{\partial^2 T}{\partial \zeta^2} + A\frac{\partial T}{\partial \zeta} + BT + C = 0 \tag{15}$$

$$A = -\frac{1}{0.148\zeta}(-2.8\times10^{-5}x^4 + 9.1\times10^{-5}x^3 - 7.5\times10^{-5}x^2 + 6.6\times10^{-6}x - 0.148)$$

$$B = -\frac{1}{0.148\zeta}(-1.11\times10^{-4}x^3 + 2.71\times10^{-4}x^2 - 1.5\times10^{-4}x + 6.6\times10^{-6})$$

$$C = -\frac{1}{0.148\zeta}(-5.85\times10^{-12}x^4 + 2.58\times10^{-11}x^3 - 3.9\times10^{-11}x^2 + 2.4\times10^{-11x} - 4.9\times10^{-12})$$

Eq. (15) is solved according to the following assumptions:

(1) The spiral groove ranges only from the root radius of the rotating ring to the outer radius. The rotating seal ring face is divided into two faces that run from the root radius to the outer radius and from the inner radius to the root radius.
(2) The temperature change is calculated from the outer radius to the root radius and then from the inner radius to the root radius.
(3) The supplied gas follows the ideal gas law.
(4) The gas flow follows laminar flow conditions.
(5) The inlet temperature of the gas film is given.
(6) A derivative with respected to the temperature at the root radius is given as zero. Figs. 7, 9 and 10 imply that the root radius region presents the maximum temperature and pressure. Thus, the root radius should indicate a turning point.

MATLAB software is used to solve Eq. (15). The temperature is plotted against the non-dimensional radius, $\zeta = r/R_i$, where r and R_i are the radial locations of interest from the inner to the outer radius of the rotating ring and the inner radius of the rotating ring, respectively (Fig. 11). Fig. 11(a) shows that temperature increases with the non-dimensional radius by approximately 0.0021 °C between the inner and root radii. Fig. 11(b) indicates that temperature decreases with increasing non-dimensional radius by roughly 0.2727 °C between the root and outer radii. Fig. 11(a) and (b)

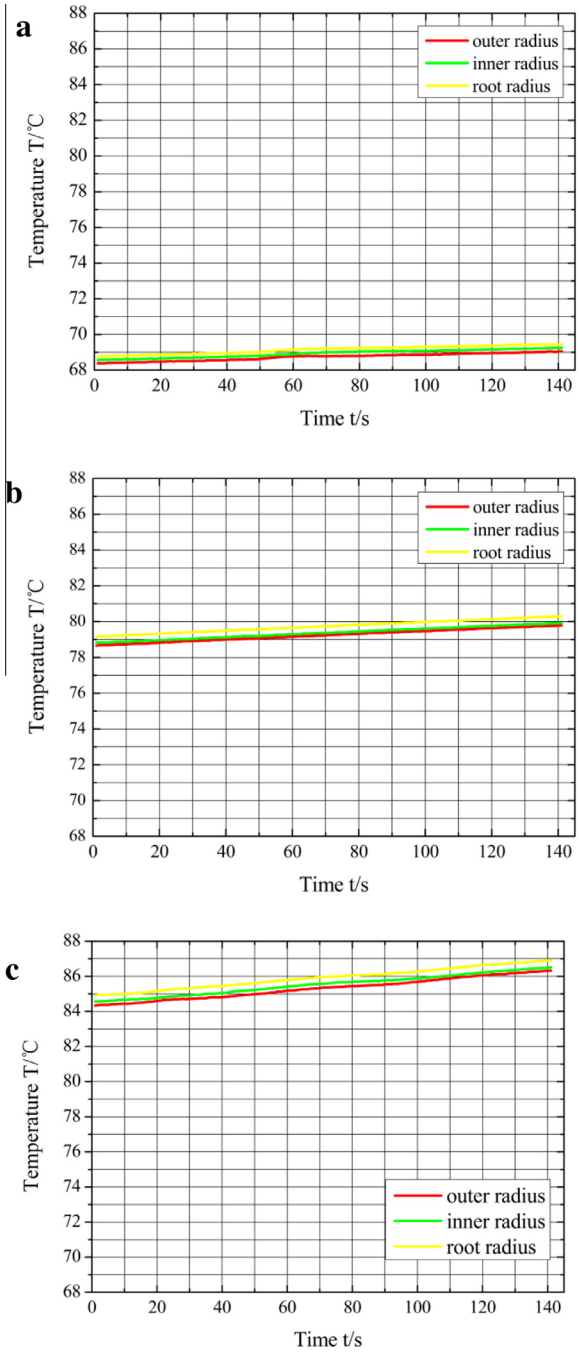

Fig. 8. Curves of temperature variation on the seal gas film for different rotating speed. (a) Temperature distribution at n = 8000 r·min^{-1}and p = 3.0 MPa. (b) Temperature distribution at n = 9000 r·min^{-1} and p = 3.0 MPa. (c) Temperature distribution at n = 10,000 r·min^{-1}and p = 3.0 MPa.

respectively illustrate the increase in interfacial temperature along the r direction before reaching a maximum value and the corresponding decrease upon peaking. The increase in temperature between the root and outer radii is more significant than that between the root and inner radii because of thermal dissipation. We applied Eq. (15) to compute the gas film temperature between the rings; this equation suggests that thermal generation is a function of the second derivative r. Thus, thermal dissipation alters the temperature along the r direction. Moreover, the temperature drop in this region is close to that on the outer surface of the rotational seal because the maximum linear velocity can facilitate the removal

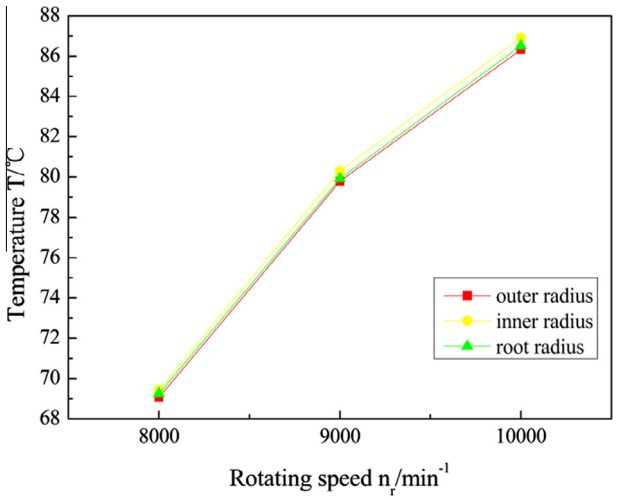

Fig. 9. Gas film temperature distribution at $n_r = 8000–10{,}000\ \mathrm{r\cdot min^{-1}}$ and $p = 3.0$ MPa.

Table 1
The values of the parameters of the seal rings and properties of the working condition.

Parameter	Name	Value
R_i	Inner radius	0.0862 m
R_o	Outer radius	0.114 m
R_r	Root radius	0.102 m
R_e	Slip radius	0.945 m
b	Seal ring face width	0.0278 m
A_s	Stationary ring area	0.017 m^2
A_e	Effective area of medium acting on the stationary ring surface	0.013 m^2
L	Axial length of stationary ring	0.0144 m
α	Spiral angle	16°
E	A half of groove depth	0.000004 m
n	Number of spiral grooves	16
p_i	Medium pressure	4 MPa
p_o	Environmental pressure	0.1013 Mpa
n_r	Rotating speed	10,000 r/min
h	Film thickness	0.000004 m
F_s	Spring force	110 N
T_0	Initial temperature	293.15 K

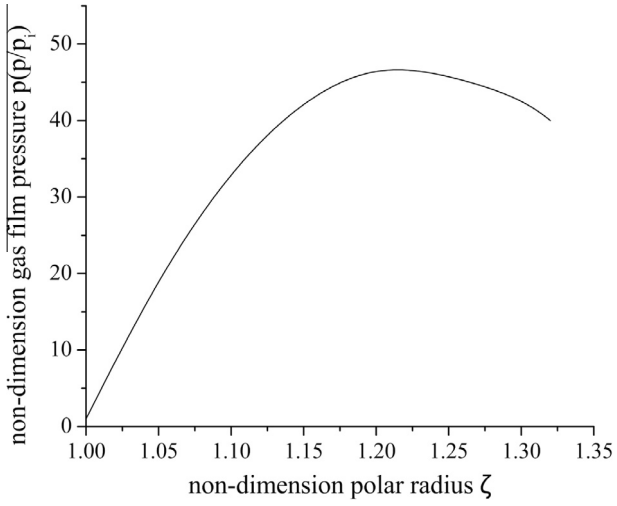

Fig. 10. Curve of non-dimensional gas film pressure p changes with the non-dimensional polar radius ζ.

Table 2
The physical constant interrelates to the dry gas seal.

Parameter	Name	Value
c_p	Specific heat of at gas constant pressure	1.0064 KJ/(kg·K)
μ	Dynamic viscosity of gas	1.8247×10^{-5} Pa·s
ρ	Gas density	1.1885 kg/m^3
λ	Heat conductivity	0.0255 W/(m·K)
σ_v	Coefficient of the adjustment in the molecular tangential momentum	1
l	Molecular free path	6.89×10^{-8} m
a	Coefficient of linear expansion for stationary ring	5.5×10^{-6} 1/K

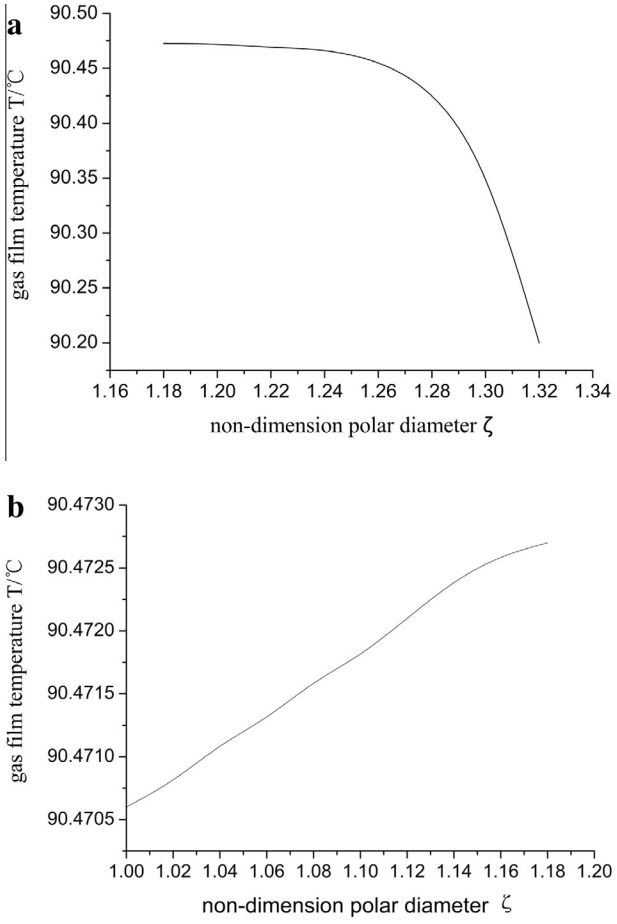

Fig. 11. Temperature curve (a) from the outer radius to the root radius and (b) from the inner radius to the root radius.

of a large amount of heat [Fig. 11(b)]. The temperature reaches roughly 90.20 °C at a location corresponding to the outer radius of the rotational ring. Nonetheless, the change rules of the temperature curves depicted in Fig. 11(a) and (b) differ. The groove area generated through the spiral groove ranges from the outer radius to the root radius of the rotating seal ring. Therefore, the pressure on the root radius is not only observed at the maximum point but also at the turning point. The increase in temperature is mainly attributed to the fact that a drop in the pressure on the root radius region facilitates thermal dissipation in the rotational ring face. The temperature distribution in this face shows the following order: root radius temperature > inner radius > outer radius.

Analytical expressions to describe the temperature ranging from the outer radius to the root radius and from the root radius

to the inner radius are determined by applying the least-square methods. The equation to determine the temperature of the rotational ring from the outer radius to the root radius is expressed as:

$$T = -3.187\zeta^4 + 13.659\zeta^3 - 21.929\zeta^2 + 15.64\zeta + 86.286 \quad (16)$$

The equation to compute the temperature from the inner radius to the root radius is written as:

$$T = -3288.352\zeta^4 + 16100.789\zeta^3 - 29559.336\zeta^2 + 24115.877\zeta - 7286.570 \quad (17)$$

Table 3 compares the experimental and theoretical data. The temperature distribution results calculated using energy equations that consider thermal dissipation are similar to the experimental results, thus suggesting that the experimental method is reliable and that the tendency of temperature can be predicted by the theoretical method. Moreover, the temperature peaks at the root radius, in agreement with both the theoretical results and test data. Thus, the proposed theory and experiment verify the maximum temperature in the groove root area. The temperature increase is attributed to thermal dissipation caused by a significant drop in pressure. Table 3 also indicates a clear difference between the theoretical results and the experimental data. This difference first increases and then decreases from the outer radius to the inner radius and is maximized at the root area of the groove. The change observed is identical to the distribution of the gas film temperature. The error rates at the root radius and inner radius of the rotating seal ring are 0.47% and 0.18%, respectively; hence, the difference between the experimental data and theoretical calculations is slight. The theoretical calculation method presented in this work can therefore be applied to analyze dry gas seal temperatures. The analysis results also show that thermal dissipation can serve as a factor influencing the optimization of groove designs.

4.3. Comparison with a seal isothermal model

It is assumed that there is not deformation under an isothermal model, but the thermo-elastic is occurred under the thermal model employed in the passage. With reference to Eqs. (16) and (17), the equation to determine the temperature of the rotational ring from the inner radius to the outer radius is expressed as:

$$T = -12750.73635\zeta^6 + 86515.08604\zeta^5 - 244270.57735\zeta^4 + 367347.97175\zeta^3 - 310334.75913\zeta^2 + 139637.43983\zeta - 26053.95523 \quad (18)$$

The equation for seal rings thermo-elastic deformation [26] is written as:

$$\delta_{ta} = aLb\Delta T/L = ab\Delta T \quad (19)$$

In the view of the seal rings materials, the deformation of the rotating ring is neglected. Thus, the equation for stationary ring thermo-elastic deformation is expressed as:

$$\delta_{ta} = ab(T - T_0) \quad (20)$$

where T is the gas film temperature; T_0 is the initial temperature; a is the coefficient of linear expansion for stationary ring; b is the width of stationary ring; L is the axial length of stationary ring.

Table 3
The experimental results and theoretical predictions for the gas film temperature.

Name	Inside radius (°C)	Root radius (°C)	Outside radius (°C)
Theoretical predictions	90.4706	90.4727	90.20
Experimental data	90.63	90.90	90.20

The structure of sealing rings affects the shape of the gas film. Thus, the film thickness h is a constant when non-deformation. However the film thickness h_b is variable value when the thermo-elastic deformation is occurred. The equation for film thickness can be expressed as:

$$h_b = h_{\min} + \Delta \quad (21)$$

$$\Delta = \delta_{ta\max} - \delta_{ta} \quad (22)$$

where $\delta_{ta\max}$ is the maximum value of stationary ring thermo-elastic deformation; $h_{\min}$ is minimum value of film thickness. The Fig. 12 presents the geometrical relationship between h_b, $h_{\min}$, Δ, $\delta_{ta\max}$ and δ.

The PH linear method is employed and combined with the iteration method for Eq. (2). The function of opening force is obtained with the following formula [23]:

$$F_o = 2\pi \int_{R_i}^{R_0} rpdr = \pi\left(R_0^2 - R_i^2\right)\left(\frac{p_i + Ep_i\left(\eta_{1(\zeta)}\cos\omega + \eta_{2(\zeta)}\cos\omega\right)/(E + h_b)}{1 - \varepsilon_z\cos\varphi - E\cos\omega/(E + h_b)} - \frac{3}{2}\beta_0[E/(E + h_b)]^2\eta_{2(\zeta)}(\zeta_0 - \zeta)p_i\right) \quad (23)$$

When the thermo-elastic deformation is occurred, the gas film and seal rings will build a new force balance. For dry gas seal, the opening force F_o must be equal to the closing force F_c during steady state operation:

$$F_o = F_c \quad (24)$$

and

$$F_c = F_p + F_e = p_iA_e + p_sA_s \quad (25)$$

where, A_e refers to effective area of medium acting on the stationary ring surface and A_s is the stationary ring area, p_s is the spring force.

The minimum value of film thickness can be obtained by substituting the Table 1 data derived with Eqs. (23) and (25) into (24) and combined with MAPLE software. The minimum value of film thickness ($h_{\min}$) is 2.14 μm.

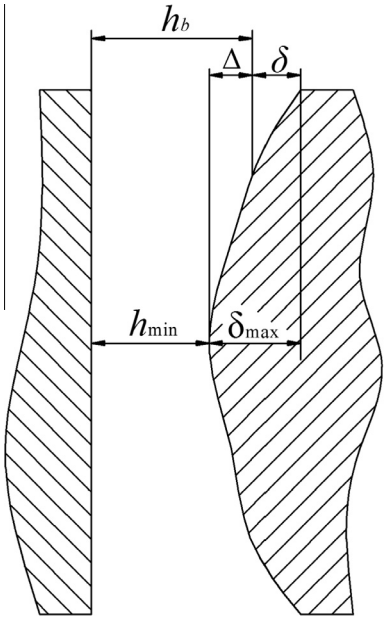

Fig. 12. The structural diagram of the film thickness.

When combined with Eqs. (18)–(20), the thermo-elastic deformation for the stationary ring can be expressed as:

$$\delta_{ta} = -1.0099 \times 10^{-3}\zeta^6 + 6.852 \times 10^{-3}\zeta^5 - 1.9346 \times 10^{-2}\zeta^4 + 2.9094 \times 10^{-2}\zeta^3 - 2.4579 \times 10^{-2}\zeta^2 + 1.1059 \times 10^{-2}\zeta - 2.0867 \times 10^{-3} \quad (26)$$

Based on Eqs. (21), (22) and (26) and combined with $h_{\min} = 2.14$ μm, the expression of film thickness is expressed as:

$$h_b = 1.0099 \times 10^{-3}\zeta^6 - 6.852 \times 10^{-3}\zeta^5 + 1.9346 \times 10^{-2}\zeta^4 - 2.9094 \times 10^{-2}\zeta^3 + 2.4579 \times 10^{-2}\zeta^2 - 1.1059 \times 10^{-2}\zeta + 2.105 \times 10^{-3} \quad (27)$$

The function of gas film pressure under the thermo-elastic deformation is obtained with the following formula:

$$P_b = \psi_2/H = 1 + \eta_b(\eta_{1(\zeta)}\cos\omega + \eta_{2(\zeta)}\sin\omega)/H - \frac{3}{2}\beta_0\eta_b^2\eta_{2(\zeta)}(\zeta_0 - \zeta) \quad (28)$$

where, $\eta_b = E/(E + h_b)$.

The expression for the radial flow of dry gas seal is written as:

$$Q = \int_0^h 2\pi v R_i dz = -\frac{(1 + 6kn')\pi p_i h_b^3}{6\mu}\frac{\partial P_b}{\partial \zeta} \quad (29)$$

The leakage flow is written as:

$$Q'|_{\zeta=1} = -\frac{(1 + 6kn')\pi}{6}\left(\frac{\partial P_b}{\partial \zeta}\right)_{\zeta=1} \quad (30)$$

When $p_i = 4$ MPa, $n_r = 10{,}000$ r/min, combined with Eqs. (3), (27), (28) and (30), the leakage flow of non-deformation and thermo-elastic deformation are calculated respectively by MAPLE software:

The leakage flow of non-deformation is 0.519 m^3/h. The leakage flow of the thermo-elastic deformation is 0.726 m^3/h. The result shows that the leakage flow of the thermal model is greater than that of an isothermal leakage. The sealing opening force of an isothermal model is 51155.70 N, and the sealing opening force of the thermal model is 65199.58 N. The sealing opening force of the thermal model is greater than the closing force. Because the gas film and the seal rings need to be built a new force balance. The film thickness becomes bigger and the opening force will decrease in the thermal model. When the film thickness becomes bigger, the leakage flow is greater because of gas film stiffness. Thus, the leakage flow of the thermal model is greater than that of an isothermal leakage. The results indicate that an isothermal model isn't good enough to predict the seal performance characteristics. It is worthwhile to develop a thermal model for the seal energy equation considered the thermal dissipation to predict the temperature fields and research the performance of dry gas seal.

5. Conclusion

This research determines temperature changes in the gas film of sealing rings. An experimental test is conducted to measure the temperature distribution in a dry gas seal, and a theoretical calculation method based on seal dynamics, energy equations, and thermal dissipation is proposed. The distributions and values of temperature are calculated at rotating speed of 10,000 r/min and a medium pressure of 4.0 MPa. The theoretical results are close to the experimental data. Besides confirming that temperature increments is attributed to thermal dissipation in the rotating ring face because of a significant drop in the pressure of the root radius region, the results also confirm the reliability of the proposed theory and experiment. Accurate measurements and theoretical calculations of gas film temperature can facilitate design recommendations, help determine the temperature distribution in seal rings, and serve as a basis for optimizing future groove designs under thermal dissipation. The theoretical calculations exhibit minimal errors because the influence of thermal dissipation alone is considered in theoretical calculations of the gas film; other thermal motions are neglected (here, friction heat, thermal dissipation, thermal convection, etc., are considered thermal motions). Future studies on gas film flow characteristics and stability of a dry gas seal system must incorporate various changes in thermal motions to enhance the reliability of the theoretical results.

Acknowledgment

This work is supported by the National Natural Science Foundation of China (Grant No. 51165020).

Appendix A. Supplementary data

Supplementary data associated with this article can be found, in the online version, at http://dx.doi.org/10.1016/j.ijheatmasstransfer.2016.01.045.

References

[1] C.H. Li, Thermal deformation in a mechanical face seal, ASLE Trans. 19 (2) (1976) 146–152.
[2] Z.G. Luan, M.M. Khonsari, Heat transfer analysis in mechanical seals using fin theory, J. Eng. Tribol. 221 (6) (2007) 717–725.
[3] J.C. Doane, T.A. Myrum, J.E. Beard, An experimental–computational investigation of the heat transfer in mechanical face seals, Int. J. Heat Mass Transfer 34 (4) (1991) 1027–1041.
[4] P. Merati, N.A. Okita, R.L. Phillips, L.E. Jacobs, Experimental and computational investigation of flow and thermal behavior of a mechanical seal, Tribol. Trans. 42 (4) (1999) 731–738.
[5] B. Tournerie, J.C. Danos, J. Frêne, Three-dimensional modeling of THD lubrication in face seals, ASME J. Tribol. 123 (1) (2001) 196–204, http://dx.doi.org/10.1115/1.1327584.
[6] N. Brunetière, B. Tournerie, J. Frêne, TEHD lubrication of mechanical face seals in stable tracking mode: Part 1-Numerical model and experiments, ASME J. Tribol. 125 (3) (2003) 608–616, http://dx.doi.org/10.1115/1.1510885.
[7] N. Brunetière, B. Tournerie, J. Frêne, TEHD lubrication of mechanical face seals in stable tracking mode: Part 2-Parametric study, ASME J. Tribol. 125 (3) (2003) 617–627, http://dx.doi.org/10.1115/1.1510886.
[8] M.T.C. Faria, W.M. Miranda, Pressure dam influence on the performance of gas face seals, Tribol. Int. 47 (3) (2012) 134–141, http://dx.doi.org/10.1016/j.triboint.2011.10.011.
[9] S. Offermann, J.L. Beaudoin, C. Bissieux, H. Frick, Thermoelastic stress analysis under nonadiabatic conditions, Exp. Mech. 37 (4) (1997) 409–413.
[10] S. Thomas, N. Brunetière, B. Tournerie, Thermoelastohydrodynamic behavior of mechanical gas face seals operating at high pressure, ASME J. Tribol. 129 (4) (2007) 841–850, http://dx.doi.org/10.1115/1.2768086.
[11] L.S. Andres, Z. Ashton, Comparison of leakage performance in three types of gas annular seals operating at a high temperature, Tribol. Trans. 53 (3) (2010) 463–471, http://dx.doi.org/10.1080/10402000903420803.
[12] S. Blasiak, P.A. Laski, J.E. Takosoglu, Parametric analysis of heat transfer in non-contacting face seals, Int. J. Heat Mass Transfer 57 (1) (2013) 22–31, http://dx.doi.org/10.1016/j.ijheatmasstransfer.2012.09.058.
[13] H. Wang, B.S. Zhu, J.S. Lin, C.L. Ye, A thermohydrodynamic analysis of dry gas seals for high-temperature gas-cooled reactor, ASME J. Tribol. 135 (2) (2013) 021701–021709, http://dx.doi.org/10.1115/1.4007807.
[14] I. Etison, I. Constaninescu, Experimental observation of the dynamic behavior of noncontacting coned-face mechanical seals, ASLE Trans. 27 (3) (1984) 263–270.
[15] H. Kasem, J.F. Brunel, P. Dufrénoy, Y. Desplanques, B. Desmet, Monitoring of temperature and emissivity during successive disc revolutions in braking, J. Eng. Tribol. 226 (9) (2012) 748–759, http://dx.doi.org/10.1177/1350650112446401.
[16] H. Kasem, J.F. Witz, P. Dufrénoy, Y. Desplanques, Monitoring of transient phenomena in sliding contact application to friction brakes, Tribol. Lett. 51 (2) (2013) 235–242, http://dx.doi.org/10.1007/s11249-013-0147-5.
[17] W.F. Huang, Y.B. Lin, Z. Gao, W.J. Fan, S.F. Suo, Y.M. Wang, An acoustic emission study on the starting and stopping processes of a dry gas seal for pump, Tribol. Lett. 49 (2) (2013) 379–384, http://dx.doi.org/10.1007/s11249-012-0077-7.
[18] W.F. Huang, Y.B. Lin, Y. Liu, X.F. Liu, Z. Gao, Y.M. Wang, Face rub-impact monitoring of a dry gas seal using acoustic emission, Tribol. Lett. 52 (2) (2013) 253–259, http://dx.doi.org/10.1007/s11249-013-0210-2.

[19] Z.G. Luan, M.M. Khonsari, Analysis of conjugate heat transfer and turbulent flow in mechanical seals, Tribol. Int. 42 (5) (2009) 762–769, http://dx.doi.org/10.1016/j.triboint.2008.10.011.
[20] Z.G. Luan, M.M. Khonsari, Heat transfer correlations for laminar flows within a mechanical seal chamber, Tribol. Int. 42 (5) (2009) 770–778, http://dx.doi.org/10.1016/j.triboint.2008.10.008.
[21] C. Visconte, M. Conte, M.C. Mattone, Analysis of the leakage path in an air-lubricated seal, Tribol. Int. 42 (6) (2009) 844–848, http://dx.doi.org/10.1016/j.triboint.2008.11.001.
[22] S. Blasiak, An analytical approach to heat transfer and thermal distortions in non-contacting face seals, Int. J. Heat Mass Transf. 81 (2015) 90–102, http://dx.doi.org/10.1016/j.ijheatmasstransfer.2014.10.011.
[23] X.X. Ding, J.J. Pu, M.J. Han, W.Z. Zhang, S.R. Yu, Calculation and analysis of gas film stiffness in the spiral groove gas seal based on the second order slip boundary, J. Mech. Eng. 47 (23) (2011) 119–124 (in Chinese). doi: 10.3901/JME.2011.23.119.
[24] J.Z. Zhang, H.P. Chang, Heat Transfer, 2rd ed., China Science Press, Beijing, China, 2009, pp. 98–100.
[25] X.X. Ding, D.L. Chen, W.Z. Zhang, S.R. Yu, Z.N. Du, Approximate calculation and parameters optimization for micro scale flow field in spiral grooved gas seals, Chin. J. Appl. Mech. 24 (3) (2007) 425–428 (in Chinese). 1000, doi: 4939(2007)03-0425-04.
[26] Gu. Yongquan, Practical Technology of Mechanical Seal, China Machine Press, Beijing, 2002, pp. 141–145.